THE ASTROPHYSICAL JOURNAL, 208:944–954, 1976 September 15

CORRELATION ANALYSES OF MICROSTRUCTURE AND NOISELIKE INTENSITY FLUCTUATIONS FROM PULSAR 2016+28

J. M. CORDES
Department of Applied Physics and Information Science, University of California, San Diego
Received 1975 March 27; revised 1976 February 16

ABSTRACT

Correlation analyses of pulses obtained at 430 MHz with 12 μs resolution show that the pulsar signal is accurately described as amplitude-modulated Gaussian noise. In the average autocorrelation function of many pulses, microstructure decorrelates at a 0.29 ms lag and is quasi-periodic with a 0.9 ms period. The microstructure in individual subpulses is usually quasi-periodic with a period that is usually in the range 0.6 to 1.1 ms. Microstructure that occasionally has periods between 0.3 and 0.5 ms tends to be weaker and is of shorter duration than the longer period microstructure.

The hypothesis of D. C. Backer that there is a pulse to pulse correlation of the microstructure along a band of drifting subpulses was tested by computing cross-correlation functions of successive subpulses. Although average cross-correlations show no evidence of any such correlation, it does appear that the period of the quasi-periodic microstructure exhibits some pulse to pulse correlation in a *few* bands of subpulses. In general, the period changes markedly from pulse to pulse and between the subpulses in the same pulse. It is therefore implausible that stellar vibration, which has a 1 ms period and a 1 s damping time for a neutron star, is the cause of microstructure periodicities.

Subject heading: pulsars

I. INTRODUCTION

Three categories of short-term temporal structure have been identified in pulsar signals. The *mean pulse profile*, obtained by averaging many pulses together, has an equivalent width of about 20 degrees of pulse longitude. Individual pulses generally show large deviations from the mean profile and are composed of *subpulses* and *micropulses* (microstructure) with typical widths of several degrees and several tenths of a degree, respectively.

To date, most of the literature has been concerned with the properties of mean pulse profiles and subpulses. Microstructure has received comparatively little attention because the typical receiver bandwidths used allow sufficient dispersion distortion to conceal microstructure. Studies of individual pulses have been concerned with subpulse time scales, modulation indices, drift properties, and polarization (e.g. Lyne, Smith, and Graham 1971; Backer 1973; Rankin, Campbell, and Backer 1974; Taylor, Manchester, and Huguenin 1975).

In order to study microstructure, dispersion distortion must be removed or observations must be made on low-dispersion pulsars at sufficiently high frequencies that distortion is minimal. Analyses of high-time resolution data include measurements of microstructure time scales by computation of intensity autocorrelation functions. Hankins's (1972) analyses of PSRs 0950+08 and 1133+16 revealed 175 μs and 575 μs microstructure time scales, respectively. Cordes and Hankins (1973) presented results for several other pulsars, including PSR 2016+28 which has a 290 μs microstructure time scale at 318 MHz. Their results also showed that (1) not all pulsars studied have microstructure, (2) when present, the microstructure time scale is frequency independent, and (3) for PSR 1919+21, microstructure exists at 74 and 111 MHz but not at 318 MHz. Boriakoff's (1973) correlation analyses verified some of these results and also revealed a quasi-periodicity, with period $P_\mu \approx 0.9$ ms, in the microstructure of PSR 2016+28.

Previous work suggests that subpulses are composed of micropulses. Hankins (1971*a*, *b*) discussed pulses of PSRs 0950+08 and 1133+16 which show micropulses as features within subpulse envelopes, although PSR 0950+08 also exhibits occasional isolated micropulses. Backer (1973) first pointed out that the microstructure of PSR 2016+28 appears to be correlated between successive pulse periods as a subpulse drifts through pulse longitude.

For signal processing purposes it is convenient to assume that subpulses and microstructure are multiplicatively related. This possibility was explored by Cordes (1975) who compared an empirical intensity model with intensity fluctuations of PSR 1919+21. The evidently accurate model represents a subpulse as a deterministic modulation of stochastic intensity variations that include microstructure. Rickett (1975) has proposed a more comprehensive model for the envelope of the undetected signal, which is referred to as amplitude-modulated noise (AMN). It depicts all pulse structures as envelopes of a complex, white Gaussian noise process whose correlation time is established by the reciprocal receiver bandwidth.

In the present paper the models of Cordes and Rickett are combined in order to explore the properties of microstructure and to test the AMN model for PSR 2016+28. The composite model is developed in the Appendix. In addition, autocorrelation functions (acf's) and cross-correlation functions (ccf's) of pulses are discussed to explore the subpulse-micropulse relationship and to test Backer's hypothesis concerning the longevity of microstructure.

II. DATA REDUCTION

Data were obtained at the Arecibo Observatory on 1973 June 26 at 430 MHz with a circularly polarized feed. The undetected signal from the 250 kHz bandwidth intermediate frequency amplifier was mixed to baseband by two local-oscillator signals whose phase difference was 90°. The resultant in-phase and quadrature signals were sampled at 4 μs intervals and written on magnetic tape. Subsequent processing at the University of California, San Diego, included removal of dispersion distortion by digital filtering (Hankins 1971*a*, *b*), detection, low-pass smoothing, and decimation in the computer to obtain 12 μs resolution.

The set of 130 pulses contained 36 bands of drifting subpulses, the general properties of which may be seen in Figures 1*a* and 1*b* where histograms of the band lengths and drift rates are shown. The drift rates were calculated from the medians of cross-correlation functions of contiguous pulses. Backer's (1973) Figure 16 shows drift rates, plotted against the running band index numbers, with the same large variability as that in the histogram. Three representative bands, numbers 2, 12, and 15 in the set of 36, are shown in Figures 1*c*, 1*d*, and 1*e*, which show prominent microstructure within the drifting subpulses. These three bands were analyzed by correlation methods to test whether or not the microstructure is correlated along a band.

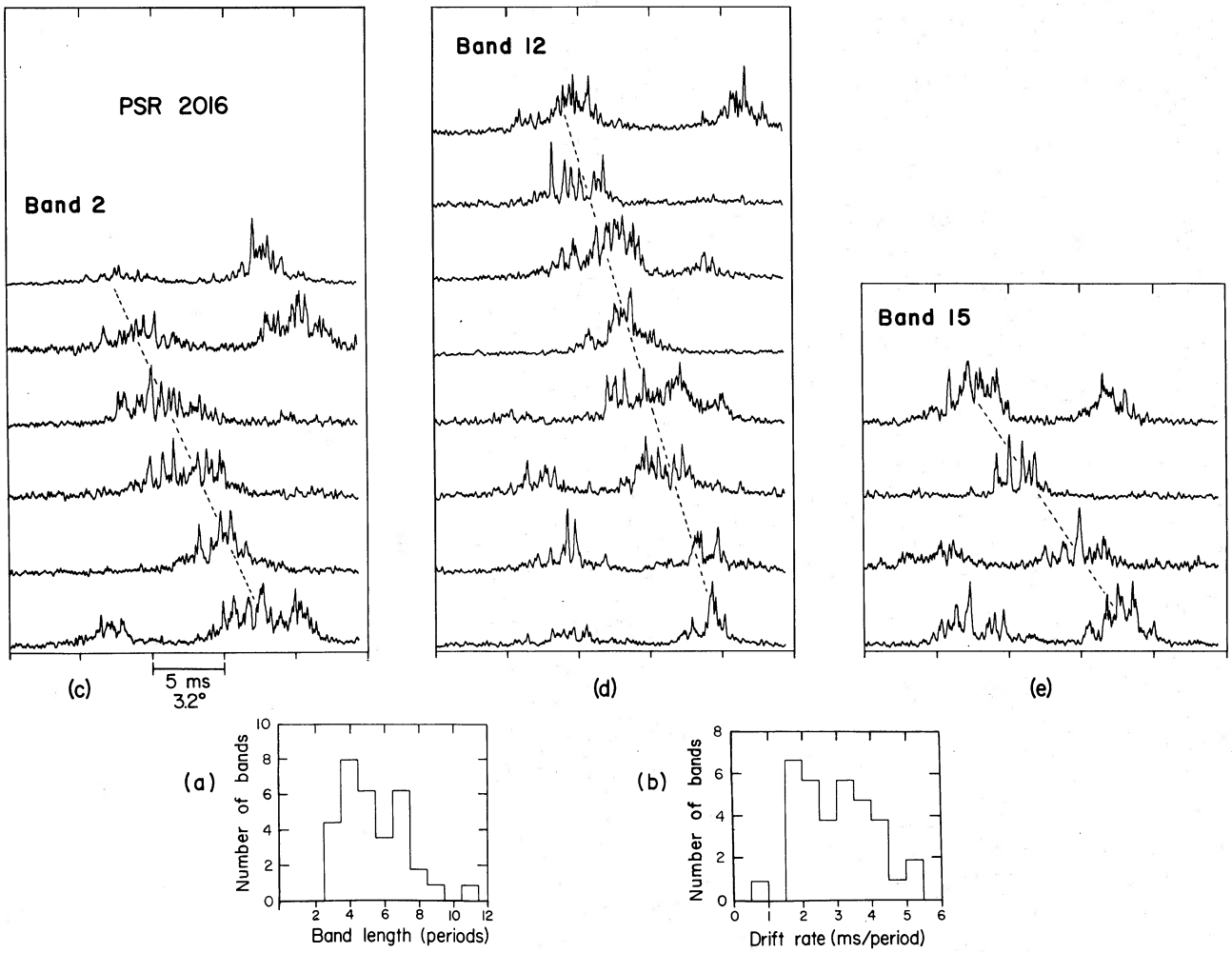

FIG. 1.—(*a*) Histogram of numbers of pulses in drifting subpulse bands. (*b*) Histogram of subpulse drift rates. (*c*, *d*, *e*) Pulses of bands 2, 12, and 15 (*dashed lines*) obtained at 430 MHz. Dispersion distortion has been removed and postdetection smoothing is 100 μs. All pulses are plotted with the same height in order that microstructure be discernible.

III. CORRELATION ANALYSIS

Intensity correlation functions of pairs of pulses were computed by multiplying discrete Fourier transforms of intensities, obtained by a Fast Fourier Transform algorithm, and transforming the product back to the time domain. Processing with N point transforms yields $N/2$ lags of the correlation function. Details of this well-known method may be found in a review by Bergland (1969).

When we denote the unnormalized correlation function of the ith and the $(i + k)$th pulses as $R_I^{(k,i)}(\tau)$, the average, normalized correlation function is obtained according to

$$r_I^{(k)}(\tau) = \sum_i R_I^{(k,i)}(\tau) \Big/ \sum_i [R_I^{(0,i)}(0) R_I^{(0,i+k)}(0)]^{1/2}, \tag{1}$$

where the $k = 0$ case is simply the autocorrelation function. The data correlation functions can be compared with those predicted by the amplitude-modulated–noise model. As shown in the Appendix, the kth correlation function is modeled as:

$$r_I^{(k)}(\tau) = r_s(\tau)[1 + m_\mu^2 \delta_{k0} \rho_\mu(\tau)][1 + \alpha' \delta_{k0} \Delta(\tau)]/(1 + m_\mu^2)(1 + \alpha'), \tag{2}$$

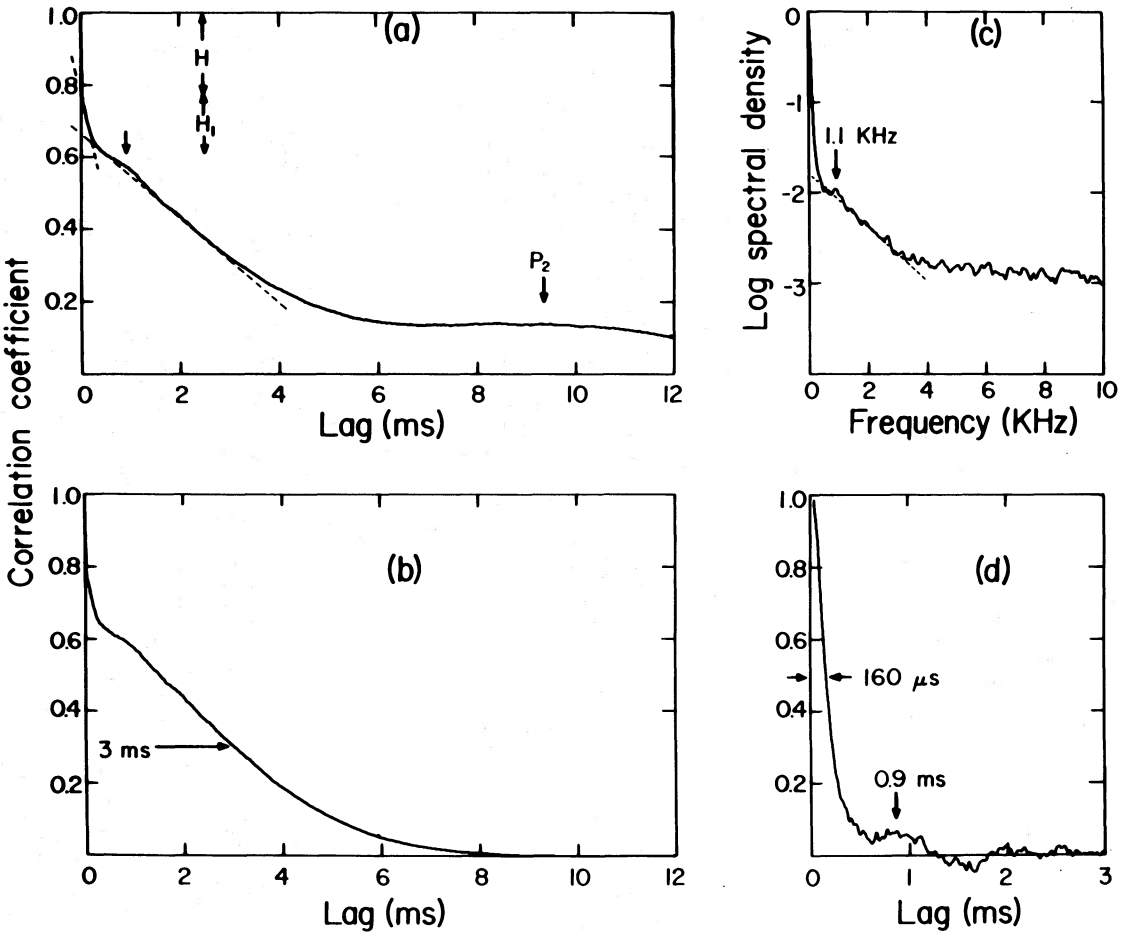

FIG. 2.—(*a*) The average autocorrelation function (acf) of 130 pulses with 12 μs resolution. All data within the pulse profile window were used in the calculation. The intersection of the dashed lines yields a 280 μs time scale for the microstructure feature. An arrow designates an enhancement at 0.9 ms lag that is due to microstructure periodicity. The enhancement at 9.5 ms, labeled P_2, is due to the occasional presence of two drifting subpulses within the pulse window. H is the height of the zero-lag spike, H_1 is a measure of microstructure strength. (*b*) The average acf computed by autocorrelating individual subpulses separately. The half-width at half-maximum of the broad portion of the acf, 3 ms, is a measure of the average subpulse time scale. (*c*) The intensity spectrum, which is the Fourier transform of the acf in Fig. 2*b*. The narrow low-frequency feature is due to subpulses. The feature at 1.1 kHz is due to microstructure periodicity. The dashed line is a fit to the microstructure portion of the spectrum used to extrapolate high frequencies to low frequencies. (*d*) The microstructure autocovariance multiplied by the subpulse autocorrelation, obtained from the spectrum in Fig. 2*c* by removal of the subpulse feature of the spectrum. The half-width at half-maximum, designated τ_μ in the text, is 160 μs.

where r_s is the acf of the subpulse modulation, ρ_μ is the normalized autocovariance (acv) of microstructure, m_μ is the microstructure modulation index (ratio of standard deviation to the mean), $\Delta(\tau)$ is a one-sample–wide spike whose properties are defined in equation (A3), δ_{k0} is the Kronecker delta, and α' is related to the noise statistics. The derivation of equation (2) assumes that subpulses modulate a microstructure random process that is statistically stationary. Subpulses are assumed to be perfectly correlated from one pulse to the next. Microstructure and noise are assumed to be completely uncorrelated between pulses, as provided for by the Kronecker deltas in equation (2). The model ignores the shape of the average-pulse profile and thus implicitly assumes that subpulses and microstructure are gated by a rectangular longitude window. The effects of this assumption will be discussed below. For details refer to the Appendix.

a) The Intensity Autocorrelation Function (acf): $k = 0$

Two average acf's were computed from the data. The first computation used all data within the window described by the average pulse profile. The second was obtained by separately autocorrelating each subpulse in the profile window. Both were normalized according to equation (1). These acf's, shown in Figures 2*a* and 2*b*, contain a wealth of information about temporal structure of the pulses. Features include (1) the zero-lag spike whose height, $H = 0.230 \pm 0.005$, is directly comparable with that predicted by the AMN model; (2) a narrow microstructure feature of width 280 μs, a time scale obtained from the intersection of two straight lines fitted to the acf; a slight enhancement of the acf at $\sim$0.9 ms, first pointed out by Boriakoff (1973), is due to the quasi-periodicity of the microstructure; (3) the microstructure feature has a height H_1 from which a value of m_μ can be obtained; (4) a wide subpulse feature has a half-height width of 3 ms; (5) a small correlation enhancement at roughly a 9.5 ms lag is P_2, the intrapulse separation of drifting subpulse bands.

The AMN model predicts that the acf has a zero-lag spike of height

$$H = (\alpha + \beta)/(\gamma^{-1} + \alpha + \beta)\,, \tag{3}$$

where β is a measure of the signal-to-(off-pulse) noise ratio, and γ is a parameter of the low pass filter. If the modulated noise of the model has complex Gaussian statistics, the detected noise will be a chi-squared random variable with two degrees of freedom whose modulation index is unity. The parameter α is the square of the modulation index, and thus $\alpha = 1$ for complex Gaussian noise. A test of the AMN model can be made by comparing the unity value of α with a value deduced from the data by solving equation (3) for α:

$$\alpha = H/\gamma(1 - H) - \beta\,. \tag{4}$$

The smoothing filter used on the data had weights proportional to the elements of the fifteenth row of Pascal's triangle, for which $\gamma = 0.145$; β was measured to be 1.04 ± 0.05; equation (4) then yields $\alpha = 1.02 \pm 0.05$, where the error is related to errors in estimates of H and β. These data are therefore consistent with noise in the AMN model having complex Gaussian statistics.

The microstructure modulation index, m_μ, can be calculated from the height of the microstructure portion of the acf, H_1, as designated in Figure 2*a*:

$$m_\mu = \{H_1^{-1}[1 + \gamma(\alpha + \beta)]^{-1} - 1\}^{-1/2}\,. \tag{5}$$

With $H_1 \approx 0.18$ we obtain $m_\mu \approx 0.50$.

In principle the microstructure autocovariance, $\rho_\mu(\tau)$, could be acquired by division of the intensity acf by $r_s(\tau)$. Although an estimate of $r_s(\tau)$ is obtainable from cross-correlations, division by it would generate large errors in the quotient because of random fluctuations in the estimate. An alternative procedure that did not rely on any auxiliary correlation function was used to obtain the product $\rho_\mu(\tau)r_s(\tau)$, a quantity that is nearly as informative as $\rho_\mu(\tau)$. The spectrum, shown in Figure 2*c*, is the Fourier transform of the acf in Figure 2*b*. The broad, subpulse acf appears as a narrow, low-frequency spectral feature and can be removed from the spectrum by extrapolating the high-frequency microstructure portion of the spectrum to the low frequencies. The extrapolation was performed by fitting an exponential to the microstructure spectrum, which appears as the straight line in the log-linear plot of Figure 2*c*. Transformation back to the time domain yields the product $\rho_\mu(\tau)r_s(\tau)$ shown in Figure 2*d*. The quasi-periodicity is revealed with a period $P_\mu = 0.9$ ms and 0.05 correlation coefficient at a 0.9 ms lag. The periodicity also appears in the power spectrum as a feature at 1.1 kHz. Also shown in Figure 2*d* are measurements of the correlation time; the half-width at half-maximum, designated τ_μ, is 160 μs and should be distinguished from the 280 μs value acquired from the intersection of lines fitted to the acf.

Autocorrelation functions of individual pulses indicate that all parameters of the microstructure vary considerably between pulse periods and between drifting subpulse bands as well. The acf's for bands 2, 12, and 15 are shown in Figure 3 with their corresponding autocovariances. Table 1 lists parameters of the microstructure for the three bands and the average over 36 bands. Of interest is the value of $\rho_\mu(\tau)$ at a lag equal to P_μ which is the height of the quasi-periodic lobe relative to the central lobe. This height is as large as 0.4 for band 15 and is zero for band 12. The average value is 0.05.

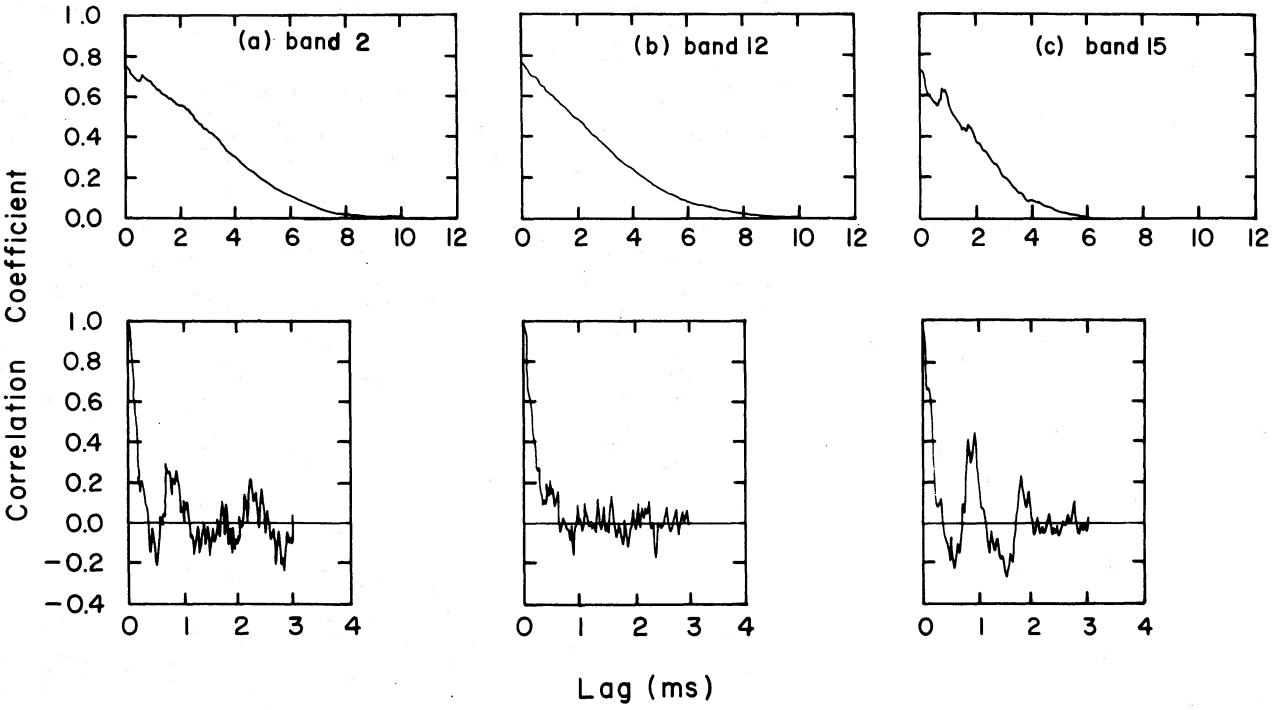

FIG. 3.—(*a, b, c*) (*upper*) The average autocorrelation functions of subpulses in drift bands 2, 12, and 15. (*lower*) The corresponding microstructure autocovariances, obtained as in Fig. 2*d*.

The acf's of individual subpulses generally show quasi-periodicities if the microstructure is strong, and often as many as 5 to 10 cycles of the periodicity are evident. About 60 percent of the subpulses show periodicities with the criterion that at least two cycles of the periodicity be discernible. A histogram of the periods in Figure 4 shows the wide range of periods. Generally, the subpulses with the strongest microstructure and the most obvious periodicities have values of P_μ that fall into the range 0.6–1.1 ms. In Figure 5 we show the acf for a pulse that has 10 cycles of a periodicity with period $P_\mu \approx 0.62$ ms. The weakness of the periodicity in the average acf is evidently due to the wide range of periods. Short-period periodicities are occasionally apparent in a range $\sim$0.3–0.5 ms; the associated microstructure tends to be weaker and narrower than the longer-period microstructure.

Along a band of drifting subpulses, P_μ usually varies over the whole range from pulse to pulse. The micropulses in band 12 have discernible periodicities in only the second through fourth subpulses with values 1.7, 0.5, and 2.2 ms, respectively. Band 2 has values over a narrower range, however: 0.81, 0.75, 0.82, 0.73, 0.70, and 0.96 ms for subpulses 1 through 6. Band 15 has the smallest variation of P_μ: 0.95, 0.96, 0.84, and 0.94 ms. Thus it appears that the mechanism that causes the microstructure periodicity may have pulse to pulse memory. For pulse periods in which there are two drifting subpulses, there does not seem to be any correlation of P_μ between the two subpulses.

b) Intensity Crosscorrelation Functions (ccf's): $k \neq 0$

Two kinds of average (over all bands) ccf's were obtained. The first was simply the sum of the ccf's for individual bands. The second was computed by finding the median, or center-of-area, of each band's ccf, shifting the ccf to center on zero lag, and then adding it to the average. The resultant ccf's are shown in Figure 6 for a one-pulse–period separation, labeled unshifted and shifted. From the unshifted ccf, an average value of the subpulse drift

TABLE 1

MICROSTRUCTURE AND SUBPULSE CORRELATION PARAMETERS

acf	τ_μ (μs)	P_μ (μs)	m_μ	τ_s (ms)	$r_s(P_\mu)\rho_\mu(P_\mu)$
Band 2.....	160 ± 10	860 ± 30	0.35 ± 0.03	3.6	0.30
Band 12.....	160	...	0.38	3.1	...
Band 15.....	160	900	0.60	2.4	0.40
Average (36 bands).....	160	900	0.55	3.0	0.05

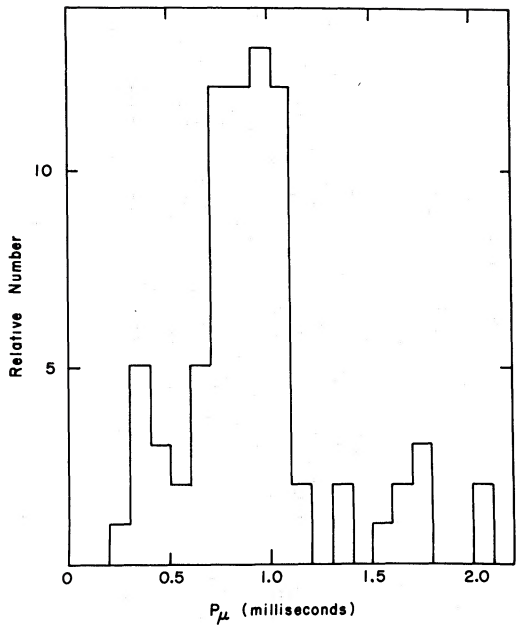

FIG. 4.—A histogram of the period P_μ of quasi-periodic microstructure

rate, 2.6 ms per period, was calculated from the ccf median. The shifted ccf is slightly narrower and has slightly greater peak correlation than the unshifted ccf. The maximum shifted correlation, 0.57, yields another estimate of m_μ from $1/(1 + m_\mu^2)(1 + \alpha') = 0.57$. The result, $m_\mu = 0.60$, is 8 percent larger than the value obtained from the acf. Similar ccf's for larger pulse-period separations have the same 0.57 peak correlation, which suggests that the discrepancy in m_μ is probably due to slight subpulse decorrelation that is induced by the mean-intensity profile, whose influence has been ignored in the analysis. Thus subpulses do not decorrelate in time (measured by pulse number) along a band. Rather, subpulses decorrelate as they drift in pulse longitude and feel the effects of the longitude-dependent pulse profile. No decrease of the ccf peak from 0.57 is observed with increasing value of k because each ccf is computed from pairs of subpulses that are distributed over all of the pulse profile; thus the effects of the average profile are integrated out as far as the ccf's are concerned.

c) *Microstructure Correlation*

Neither of the ccf averages in Figure 6 shows any microstructure feature that is similar to the acf feature. Thus either microstructure is not correlated between pulses or the averaging processes obliterate a feature that is there.

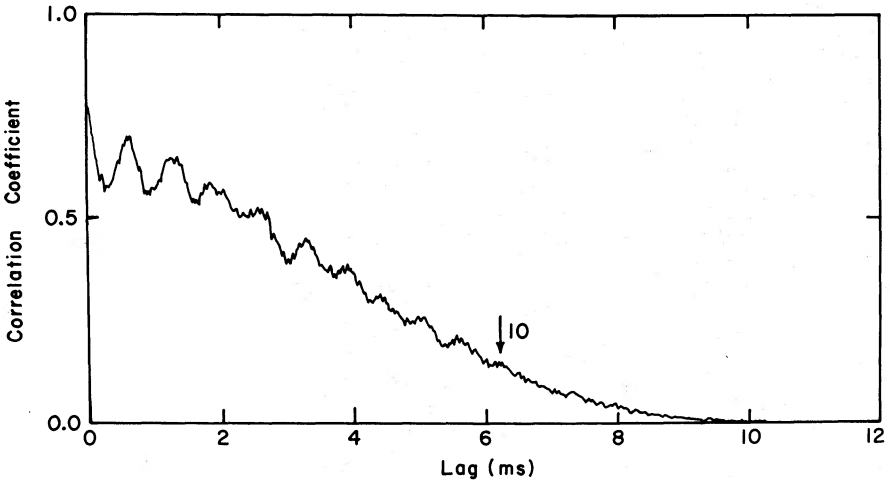

FIG. 5.—The autocorrelation function of a single pulse that has quasi-periodic microstructure with period $P_\mu = 0.624 \pm 0.02$ ms. The tenth cycle of the periodicity in the acf is indicated by the arrow.

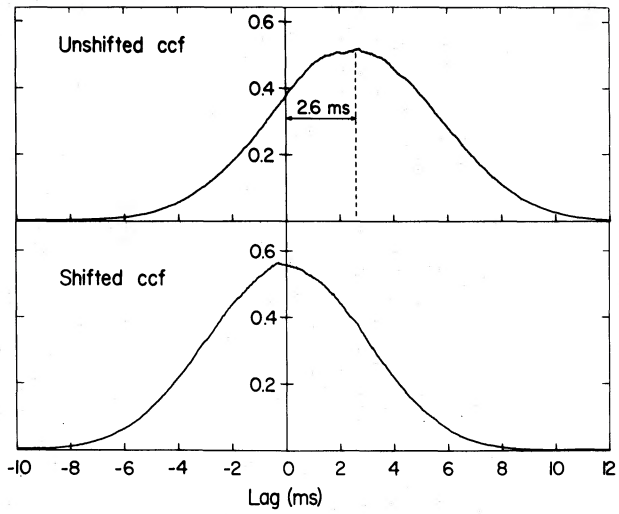

FIG. 6.—(*upper*) The average cross-correlation function (ccf) of subpulses separated by one pulse period, computed by simple averaging of ccf's of individual bands. (*lower*) The average ccf for one pulse period computed by first shifting individual band ccf's according to their median lags.

To test the hypothesis of pulse-to-pulse correlation of microstructure, ccf's for individual subpulse bands must be considered. The ccf's of bands 2, 12, and 15 are shown in Figure 7 for 1, 2, and 3 pulse-period lags. The ccf's for bands 2 and 15 show quasi-periodic fluctuations with period $P_\mu \approx 0.9$ ms, while those for band 12 show structureless fluctuations.

One step in testing whether or not microstructure is correlated is to compare the amplitudes of ccf ripples with those predicted by the intensity model. Any ccf computed from a finite number of pulses will contain fluctuations with microstructure time scales, even if microstructure is uncorrelated. The amplitudes of the fluctuations are estimated in equation (A20) in terms of m_μ, τ_μ, and τ_s assuming that microstructure is aperiodic or that periodicities in different pulses are incommensurate. When we used values of these parameters particular to each band, error limits corresponding to 2 σ were computed for the peak correlation region of the ccf's. Referring to Figure 7, it

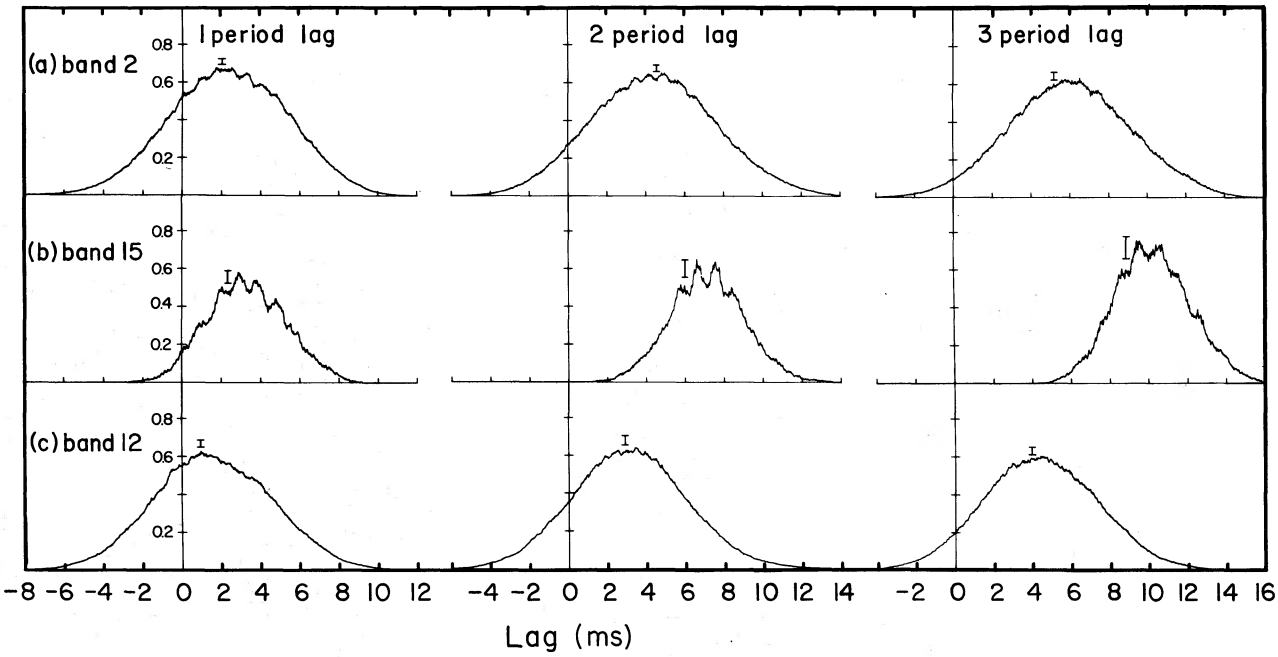

FIG. 7.—(*a*, *b*, *c*) Cross-correlation functions of pulses in subpulse bands 2, 15, and 12 for 1,2, and 3 pulse period lags. The error bars (2 σ) represent expected ripple amplitudes calculated from a model that assumes microstructure is aperiodic and strictly uncorrelated between pulse periods.

can be seen that the fluctuations for band 12 are well within the error limits, those for band 2 are marginal, while those for band 15 are larger than the limits, albeit by a small amount.

If the subpulses in a drift band contain quasi-periodic microstructure with the same period, then different error limits on the ccf ripple must be considered. The size of the ripples will depend on if the *phase* of the periodicity with respect to the centroid of the subpulse is correlated between pulse periods. If so, then the ccf ripples will have about the same amplitude as the size of the lobe at lag P_μ in the acf. If not, ripples in a ccf that is the average of several single-pair ccf's should be smaller than the acf lobe, and the ripples will not show a clear periodicity.

In Figure 7 we see that the ripples in the ccf's for bands 12 and 15 are indeed of the same amplitude as the acf lobe. Any conclusions based on this evidence must be drawn carefully because the ccf's are sums of only a few pulse-pair ccf's (for band 15 the ccf for a three-period lag was computed from only one pair of pulses).

Finally, we point out additional evidence that the phase of the microstructure periodicity might be correlated between pulse periods. In Figure 7 arrows designate the medians (the centers of area) of the ccf's. For band 15 it appears that in all three ccf's, a low point in the ripple is consistently close to the median, suggesting that the phase of the ripple in the subpulse is maintained over several pulse periods.

We hesitate to conclude with any great confidence that the phase of the microstructure periodicity is "rigidly" attached to the drifting subpulse over several pulse periods' duration. Any such rigidity implies a resonance Q of at least $P_1/P_\mu \approx 557$ ms/0.9 ms ≈ 600. Obviously, a larger sample of pulses with more sophisticated statistical tests is required to make any strong conclusion on this very important question.

IV. DISCUSSION AND CONCLUSIONS

We conclude that microstructure is weakly correlated from pulse to pulse in the sense that it can be quasi-periodic with a period that is maintained for several stellar rotations. Moreover, the data *suggest* that the reference phase of the quasi-periodicity is attached to the drifting subpulses and also may be correlated from between pulse periods. In general, however, microstructure is uncorrelated between successive subpulses and between subpulses within the same pulse.

If radio emission from pulsars is due to curvature radiation from the polar region of a skewed dipolar magnetic field, then any pulse to pulse memory of microstructure, as well as of subpulses, must be in the current injection process; the radiating particles themselves escape from the velocity of light cylinder in less than a rotation period. It is tempting to associate the ~ 0.9 ms period of quasi-periodic microstructure with stellar vibrations which have similar periods and are damped on 1 s time scales due to gravitational radiation (Cameron 1970). This interpretation is implausible, however, because the microstructure period is not the same between neighboring subpulses whose separation is ~ 10 ms.

It is well known that pulsar radiation must be due to coherent processes because of the high inferred brightness temperatures of the radiation ($\lesssim 10^{31}$ K). That the signal for PSR 2016+28 conforms to pulse-modulated Gaussian noise implies that the radiation is incoherently added before it is recorded. Incoherent addition occurs in a receiver system with bandwidth $\Delta\nu$ because the signal is convolved in the time domain with a function of width $(\Delta\nu)^{-1}$. Interstellar scattering adds radiation over a time $T_{\rm iss}$ because of differential propagation times. Incoherent addition may also occur in the pulsar if many independent emission regions contribute to the instantaneous signal.

To facilitate discussion of the noise statistics, we shall characterize the intrinsic wide-band pulsar radiation as amplitude-modulated shot noise. Shot noise (Papoulis 1965) is a sequence of narrow pulses whose occurrence times are Poisson distributed with mean density η which has units of inverse time. The spectrum of pulsar radiation typically extends to a few times 10^9 Hz and is thought to be related to the size of bunches of particles. A single bunch will radiate a shot pulse whose duration is on the order of a nanosecond, the inverse of 10^9 Hz, and thus we consider the radiation to be a sequence of shot pulses.

It can be shown (Cordes 1976) that the modulation index of shot noise (without any amplitude modulation) in a narrow-band receiver is

$$m_n = (1 + \langle a_n^4\rangle/\langle a_n^2\rangle^2\eta\Delta)^{1/2}, \tag{6}$$

where a_n is the amplitude of a shot pulse. Since the intensity is proportional to the square of the number of particles in a bunch (N_c), we have $a_n^2 \propto N_c^2$. The number of incoherent additions in the receiver resolution time is $N_i \approx \eta\Delta$. Thus a unity value of m_n, which applies to Gaussian statistics, requires that

$$\langle N_c^4\rangle/\langle N_c^2\rangle^2 N_i \ll 1 \tag{7}$$

or that

$$\sigma_{N_c^2}/\langle N_c^2\rangle \ll N_i^{1/2} \tag{8}$$

where $\sigma_{N_c^2}$ is the typical variation of the square of the number of particles in a bunch.

For the case of PSR 2016+28 at 430 MHz, $T_{\rm iss} \approx 2$ μs, a value calculated from the measurements at various frequencies of the scintillation decorrelation bandwidth (Sutton 1971). Thus the relevant time scale for considering

incoherent addition is the effective receiver resolution of 12 μs because it is larger than $T_{\rm iss}$. It is possible that wide bandwidths and high frequencies (such that $T_{\rm iss}$ is small) would reveal a violation of equation (7) and therefore provide information on the number of particles in a bunch. However, it is also possible that the shot noise density may be so large, due to the particle environment in the emission region, that equation (7) is always satisfied.

I would like to thank T. H. Hankins for his discussions and guidance with the observations. Helpful discussions with W. A. Coles and B. J. Rickett are also gratefully appreciated. This work was supported by the NSF through grant MPS 71-03377-A02. The National Astronomy and Ionosphere Center, Arecibo Observatory, is operated by Cornell University under contract with the National Science Foundation.

APPENDIX

CORRELATION FUNCTIONS OF AMPLITUDE MODULATED NOISE

The amplitude-modulated noise (AMN) model formulated by Rickett (1975) is a statistical representation for the undetected narrow-band pulsar signal after dispersion distortion has been removed. Hankins (1971) and Rickett (1975) have described in detail the data acquisition and dispersion removal techniques. Basically, the signal from the receiver with center frequency ν_0 and bandwidth $\Delta\nu$ is shifted to zero center-frequency. The resultant signal has bandwidth $\Delta\nu/2$ and is complex: in-phase and quadrature components of the signal are required for its complete description. A complex dispersion-removal filter is then applied to the baseband signal to obtain the signal of interest.

The complex signal is not statistically stationary; the AMN model represents it as the product of stationary and unstationary parts:

$$y(t) = a(t)n(t)\,, \tag{A1}$$

where $a(t)$ is a real stochastic amplitude function and $n(t)$ is complex, zero-mean, white Gaussian noise. The statistics of $n(t)$ are described by the two second moments

$$\langle n(t)n(t+\tau)\rangle = 0\,, \qquad \langle n(t)n^*(t+\tau)\rangle = \sigma_n{}^2\Delta(\tau) \tag{A2}$$

where the asterisk denotes complex conjugation and $\Delta(\tau)$ has the properties

$$\Delta(0) = 1\,, \qquad \int d\tau\Delta(\tau) = \Delta\,, \tag{A3}$$

$\Delta(\tau)$ is the autocorrelation function of the noise process; it has a width Δ and is the autocorrelation of the impulse response of the receiver. It is assumed that sampling is at the Nyquist rate, such that the sample interval, Δ, is equal to the reciprocal bandwidth. These properties of $\Delta(\tau)$ allow use of continuous functions while retaining the properties of sampled data.

The detected signal is the intensity

$$I(t) = A(t)N(t)\,, \tag{A4}$$

where $A(t) = a^2(t)$ and $N(t) = |n(t)|^2$. Separate realizations of this random process will be treated as individual pulses in correlation analyses. The ensemble-average correlation function of the ith and $(i+k)$th realizations is defined as

$$R_I{}^{(k)}(\tau) = \left\langle \frac{1}{T}\int_0^T dt I_i(t+\tau)I_{i+k}(t) \right\rangle\,, \tag{A5}$$

where the angular brackets denote ensemble average. The normalized correlation function is

$$r_I{}^{(k)}(\tau) = R_I{}^{(k)}(\tau)/R_I(0)\,. \tag{A6}$$

Note that the superscript is suppressed in the $k = 0$, or autocorrelation, case. We will also consider acf's of other functions, $f(t)$, which will be denoted $R_f(\tau)$ and will be defined as in equation (A5) with $k = 0$.

The amplitude function, $A(t)$, contains contributions from subpulse and micropulse intensity variations. $A(t)$ will be modeled as the product of a nonstationary subpulse part, $S(t)$, and a stationary microstructure part, $\mu(t)$:

$$A(t) = S(t)\mu(t)\,. \tag{A7}$$

It is convenient to describe $\mu(t)$ by its modulation index, m_μ, and its autocovariance (acv), $\rho_\mu(\tau)$, the latter being the acf of only the varying portion, $\mu(t) - \langle\mu(t)\rangle$. With m_μ defined by

$$m_\mu^2 = [\langle\mu^2(t)\rangle - \langle\mu(t)\rangle^2]/\langle\mu(t)\rangle^2 , \tag{A8}$$

the acf of $\mu(t)$ can be written as

$$r_\mu(\tau) = (1 + m_\mu^2\rho_\mu(\tau)/(1 + m_\mu^2) . \tag{A9}$$

To obtain a final expression for the correlation functions, it will be assumed that subpulses are perfectly correlated, and the microstructure and noise uncorrelated, between different realizations. Thus we obtain

$$r_I^{(k)}(\tau) = r_s(\tau)[1 + m_\mu^2\delta_{k0}\rho_\mu(\tau)][1 + \alpha'\delta_{k0}\Delta(\tau)]/(1 + m_\mu^2)(1 + \alpha') , \tag{A10}$$

where δ_{k0} is the Kronecker delta, $r_s(\tau)$ is the subpulse acf, and α' is related to the signal's noise statistics, as discussed below.

a) The Intensity Autocorrelation

Before a comparison of the model with the data can be made, the effects of smoothing and additive noise must be considered. If the intensity is smoothed by convolution with an impulse response, $h(t)$, which is defined to have unit area

$$\int dth(t)/\Delta = 1 , \tag{A11}$$

the mean intensity is unchanged but the variance is reduced by a factor $\gamma \leq 1$:

$$\gamma = \int dth^2(t)/\Delta . \tag{A12}$$

The undetected signal is contaminated by additive system noise whose statistics can be measured from off-pulse data. A parameter of interest is the intensity signal-to-noise ratio integrated over the mean intensity profile:

$$\xi = T^{-1}\int_0^T dt\langle I(t)\rangle/\langle I_{\rm off}\rangle \tag{A13}$$

where $\langle I_{\rm off}\rangle$ is the off-pulse mean intensity. The analysis assumes that the off-pulse mean has been subtracted to obtain $I(t)$. The off-pulse noise contributes only a zero-lag spike to the intensity acf, whose height is, if there is no smoothing,

$$\beta = \langle I_{\rm off}\rangle^2(1 + 2\xi)/R_{\rm A}(0) . \tag{A14}$$

If data are smoothed, the spike height is reduced by a factor γ. With these definitions the parameter α' in equation (A10) can be written as

$$\alpha' = \gamma(\alpha + \beta) , \tag{A15}$$

where $\alpha = 1$ for complex Gaussian noise.

The intensity acf thus contains a zero-lag spike of height

$$H = \alpha'/(1 + \alpha') . \tag{A16}$$

The AMN model can be tested by comparing the predicted height with that in correlation functions of data. Equivalently, a value of α estimated from the data

$$\alpha = H/\gamma(1 - H) - \beta \tag{A17}$$

can be compared with the unity value of the model.

b) Intensity Crosscorrelations

The model thus developed predicts that the ensemble average ccf's are the same for any $k \neq 0$. With $k = 1$, for example, we have

$$r_I^{(1)}(\tau) = r_s(\tau)/(1 + m_\mu^2)(1 + \alpha') . \tag{A18}$$

Subpulse drift has not been explicitly included because it merely shifts the ccf to a central lag of Dk, where D is the drift rate in time-per-pulse periods. The ccf's readily yield the microstructure modulation index from the maximum correlation.

The model ccf's are to be compared with estimates of ccf's from a finite number of pulses. The estimated ccf's will contain fluctuations due to the stochastic variations of intensity. Since the ultimate goal of the analysis is to decide whether or not microstructure is correlated between successive pulses, a comparison should be made between the ccf fluctuations in the data with those predicted by the model. To this end, we compute the ccf variance as a function of τ:

$$[\sigma_{R_k}(\tau)]^2 = T^{-1}\int_0^T dt\,[I_i(\tau)I_{i+k}(t+\tau) - R_I^{(1)}(\tau)]^2/[R_I(0)]^2\,. \tag{A19}$$

Of special interest is the zero-lag variance due to microstructure fluctuations only. If we assume that $S(t)$ is deterministic, that the width of $\rho_\mu(\tau)$ is much narrower than that of $S(t)$, and that $m_\mu^2 \ll 2$, the zero-lag microstructure variance can be estimated from

$$[\sigma_{R_k}(0)]_\mu^2 = m_\mu^2\tau_\mu/2^{1/2}(1+m_\mu^2)(1+\alpha')\tau_s\,, \tag{A20}$$

where τ_μ and τ_s are representative widths of the microstructure and subpulse acf's. If the ccf is estimated from n pairs of pulses, the variance is reduced by a factor n^{-1}.

REFERENCES

Backer, D. C. 1973, *Ap. J.*, **182**, 245.
Berland, G. D. 1969, *IEEE, Spectrum*, **6**, 41.
Boriakoff, V. 1973, Ph.D. thesis, Cornell University.
Cameron, A. G. W. 1970.
Cordes, J. M. 1975, *Ap. J.*, **195**, 193.
———. 1976, *ibid.*, in press.
Cordes, J. M., and Hankins, T. H. 1973, *Bull. AAS*, **5**, 18.
Hankins, T. H. 1971*a*, *Ap. J.*, **169**, 487.
———. 1971*b*, Ph.D. thesis, University of California, San Diego.
———. 1972, *Ap. J. (Letters)*, **177**, L11.
Lyne, A. G., Smith, F. G., and Graham, D. A. 1971, *M.N.R.A.S.*, **153**, 337.
Papoulis, A. 1965, *Probability, Random Variables and Stochastic Processes* (New York: McGraw-Hill).
Radhakrishnan, V., and Cooke, D. J. 1969, *Ap. Letters*, **3**, 225.
Rankin, J. M., Campbell, D. B., and Backer, D. C. 1974, *Ap. J.*, **188**, 609.
Rickett, B. J. 1975, *Ap. J.*, **197**, 185.
Sutton, J. M. 1971, *M.N.R.A.S.*, **155**, 51.
Taylor, J. H., Manchester, R. N., and Huguenin, G. R., 1975, *Ap. J.*, **195**, 513.

Note added in proof.—A paper by V. Boriakoff recently (August 15) appeared in *Ap. J. (Letters)* which also discusses the microstructure of pulsar 2016+28.

J. M. Cordes: Department of Physics and Astronomy, University of Massachusetts, Amherst, MA 01002